

Nanocrystals of CuMSnS_4 ($M = \text{In}$ or Ga) for Solar Energy Conversion Applications

Karthik Ramasamy,^{a*} Pravin S. Shinde,^{b,c} Nariman Naghibolashrafi^b, Shanlin Pan,^{b,c} and Arunava Gupta^{b,c*}

Supporting Information

^a UbiQD, Inc, 134 Eastgate Dr. Los Alamos, NM-87544. karthik@ubiqd.com

^b Department of Chemistry & Biochemistry, The University of Alabama, Tuscaloosa, AL-35487

^c Center for Materials for Information Technology, The University of Alabama, Tuscaloosa, AL-35487. agupta@mint.ua.edu

Electronic Supplementary Information (ESI) available: [details of any supplementary information available should be included here]. See DOI: 10.1039/x0xx00000x

Materials and Methods

Synthesis of wurtzite CuMSnS₄ (M = In or Ga) nanocrystals.

For the synthesis of wurtzite phase CuMSnS₄ (M = In or Ga) NCs, a 1:1:1 ratio of acetylacetonate complexes of copper (II) (Cu(acac)₂, 99.99+ %, 0.2 mmol), indium (III) (In(acac)₃, 0.2 mmol) or gallium (III) (Ga(acac)₃, 0.2 mmol) and tetrahydrofuran adduct of tin (IV) chloride (SnCl₄.THF, 0.2 mmol) were dispersed in oleylamine and deaerated at room temperature for 15-30 min. The dispersion was heated to 150 °C (heating rate, 16 °C/min) in nitrogen atmosphere and a mixture of *n*-dodecanethiol (*n*-DDT, 1 mL) and *tert*-dodecanethiol (*t*-DDT, 1 mL) was rapidly introduced into the reaction mixture at this temperature. The entire mixture was reheated to 210-215 °C and maintained at this temperature for 10 to 30 min. The mixture was then cooled and separated via precipitation and redispersion method using ethanol and hexane to obtain the final NC product. A similar synthesis procedure was carried out for obtaining the tetragonal phase of CuMSnS₄ (M = In or Ga) NCs but using sulfur powder dissolved in oleylamine as the sulfur source.

Phase transformation from wurtzite to tetragonal. The wurtzite phase CuMSnS₄ (M = In or Ga) NCs could be transformed to pure tetragonal phase by simple annealing of the powder sample at 400 - 450 °C for 2 - 2.5 h under N₂ atmosphere in a tube furnace.

Nanocrystals Thin Film Preparation. Nanocrystals thin films were spray coated on Mo-coated soda-lime glass substrates by spray deposition method. As an example, the spray suspension solution was prepared by dispersing 100 mg of wurtzite CuGaSnS₄ NCs in 10 mL of hexane. Few drops of oleylamine were added to stabilize the suspension before spraying it on Mo substrate with the help of a spray gun. The wurtzite CuGaSnS₄ film was annealed at 375 °C for 30 min (ramped at 5°C min⁻¹) under N₂ atmosphere. Figure 5a and 5b shows the top and cross-sectional SEM (JEOL 7000 FESEM) view of wurtzite CuGaSnS₄ thin film deposited on Mo substrate, respectively. The surface morphology of Wurtzite CuGaSnS₄ film is continuous without any pin-holes or cracks. Magnified SEM image clearly shows the size of the particles to be in the range of 10-20 nm. The cross-sectional SEM view reveals a film thickness of ~620 ±20 nm.

Characterization. Routine transmission electron microscopy (TEM) imaging was performed using a FEI-Tecnai, 300 kV transmission electron microscope equipped with a CCD camera for scanning transmission electron microscopy (STEM), a high-angle annular dark field (HAADF) detector, and energy-dispersive scanning transmission electron microscopy x-ray (EDX) spectroscopy. Scanning transmission electron microscopy (STEM) high-angle annular dark field imaging and EDX elemental mapping were performed using a FEI Company Titan G2 80-200 TEM/STEM operated at 200 kV and equipped with the X-FEG (an ultra-stable high-brightness Schottky FEG source), Super-X EDX detector system (4 windowless silicon drift detectors with a combined solid angle of 0.7 sr), and a spherical aberration corrector (CEOS DCOR) on the probe-forming optics. TEM image non-linear processing - Fourier filtering - was carried out using Gatan Digital Micrograph version 3.4. Powder X-ray diffraction (XRD) patterns and small angle X-ray

scattering (SAXS) were recorded on a Rigaku Smart Lab II instrument equipped with Cu K α radiation source operated at 40 kV and 44 mA. Samples for powder XRD measurements were covered with Paratone-N crystallographic oil to prevent excessive oxidation and deposited on the horizontal glass slide. Samples for SAXS were dissolved in hexane and the solution was loaded into 0.7 mm boron glass capillaries for measurements. PDXL v2.0 and NANO-Solver v3.5 software packages from Rigaku were used to process the powder XRD and SAXS data, respectively. SAXS data were modelled as Gamma distribution of spherical particles with normalized dispersion, σ , referred to as '*size distribution*': $\sigma[\%] = (\langle\delta R^2\rangle/\langle R\rangle^2)^{1/2}100\%$.

XPS measurements were performed using a Kratos Axis Ultra DLD instrument with base pressures less than 5×10^{-9} Torr. Samples for XPS were mounted onto a sample holder in a glove box and briefly (< 5 sec) exposed to air during transfer from the glove box to the instrument. XPS was performed with a monochromatic Al K α (1486.7 eV) source operated at 150 W with an elliptical spot size of 300 x 700 microns. Survey spectra were recorded with an 80 eV pass energy, 600-700 meV step sizes, and 100 ms dwell time. High resolution spectra were recorded with a 20 eV pass energy, 50 meV step sizes, and 100 ms dwell times. Charge neutralization was used for all samples to reduce differential charging effects. Data processing was performed with CasaXPS Version 2.3.15. Spectra were adjusted to align the C 1s peak to 284.6 eV. Absorption measurements were carried out using a Cary 6000i dual-beam UV-Vis-NIR spectrometer.

The photoconductivity response of thin film device was measured using a Keithley 2420 source meter (Keithley Instruments, Inc.) under white light illumination (AM 1.5G, 100 mW cm $^{-2}$, Xenon lamp) with the help of a solar simulator in air at room temperature and using GG495 IR light transmitting filter.

The measured photocurrent was converted to obtain the incident photon-to-light conversion efficiency (IPCE, %) using the actual power density of each monochromatic light according to a relation below:

$$IPCE (\%) = \frac{\text{No. of electrons generated}}{\text{No. of incident photons}} \times 100 = \frac{1240 \times J_{ph}}{\lambda \times P_{in}} \times 100,$$

where J_{ph} is the photocurrent density, λ is the wavelength of monochromatic light, and P_{in} is power density of incident monochromatic light.

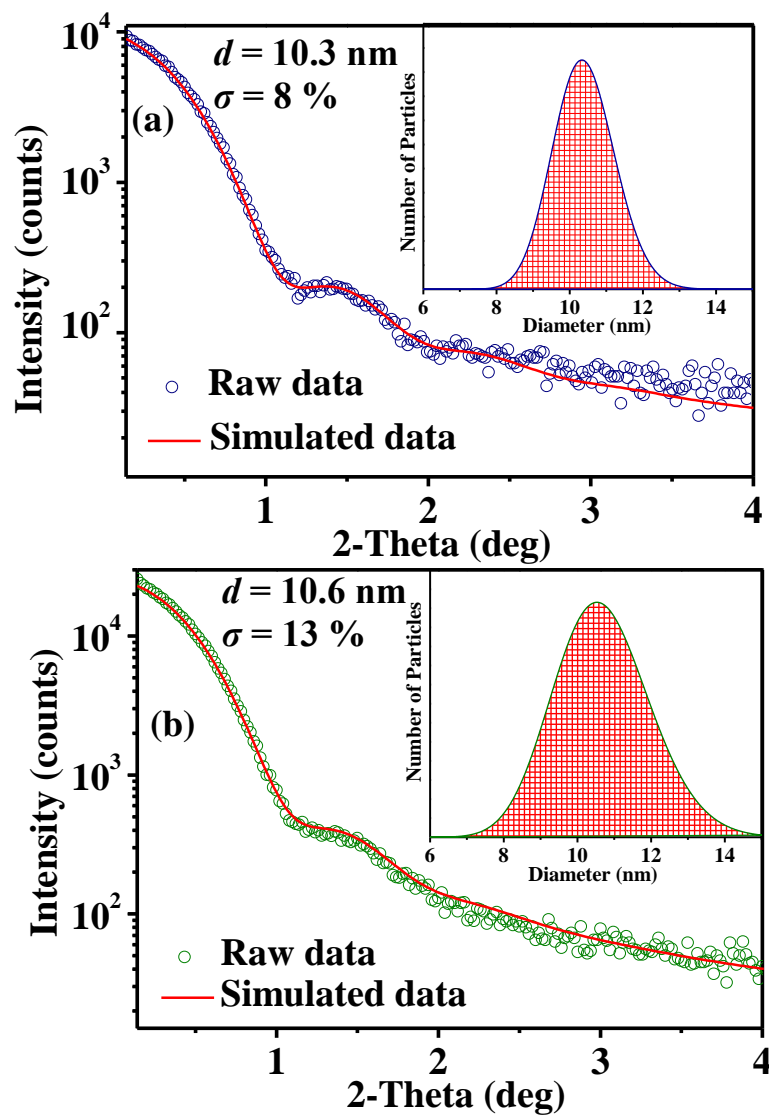


Fig. S1 (a) Small angle X-ray scattering patterns (log scale) of (a) CuInSnS₄ and (b) CuGaSnS₄ nanocrystals dispersed in hexane (Insets: particle size distribution obtained from SAXS measurements).

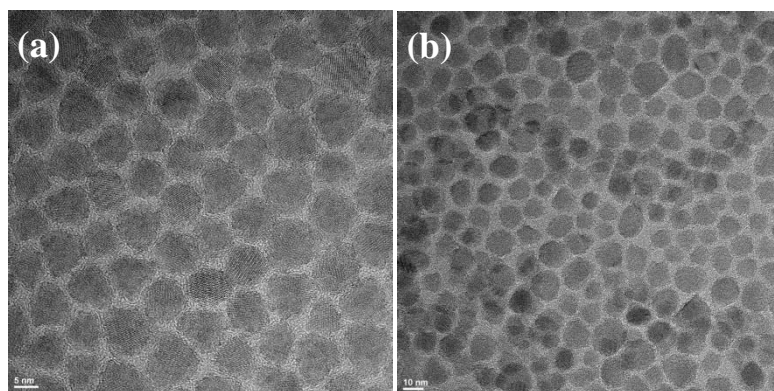


Fig S2. TEM images of defect chalcopyrite phase (a) CuInSnS_4 (b) CuGaSnS_4 nanocrystals.

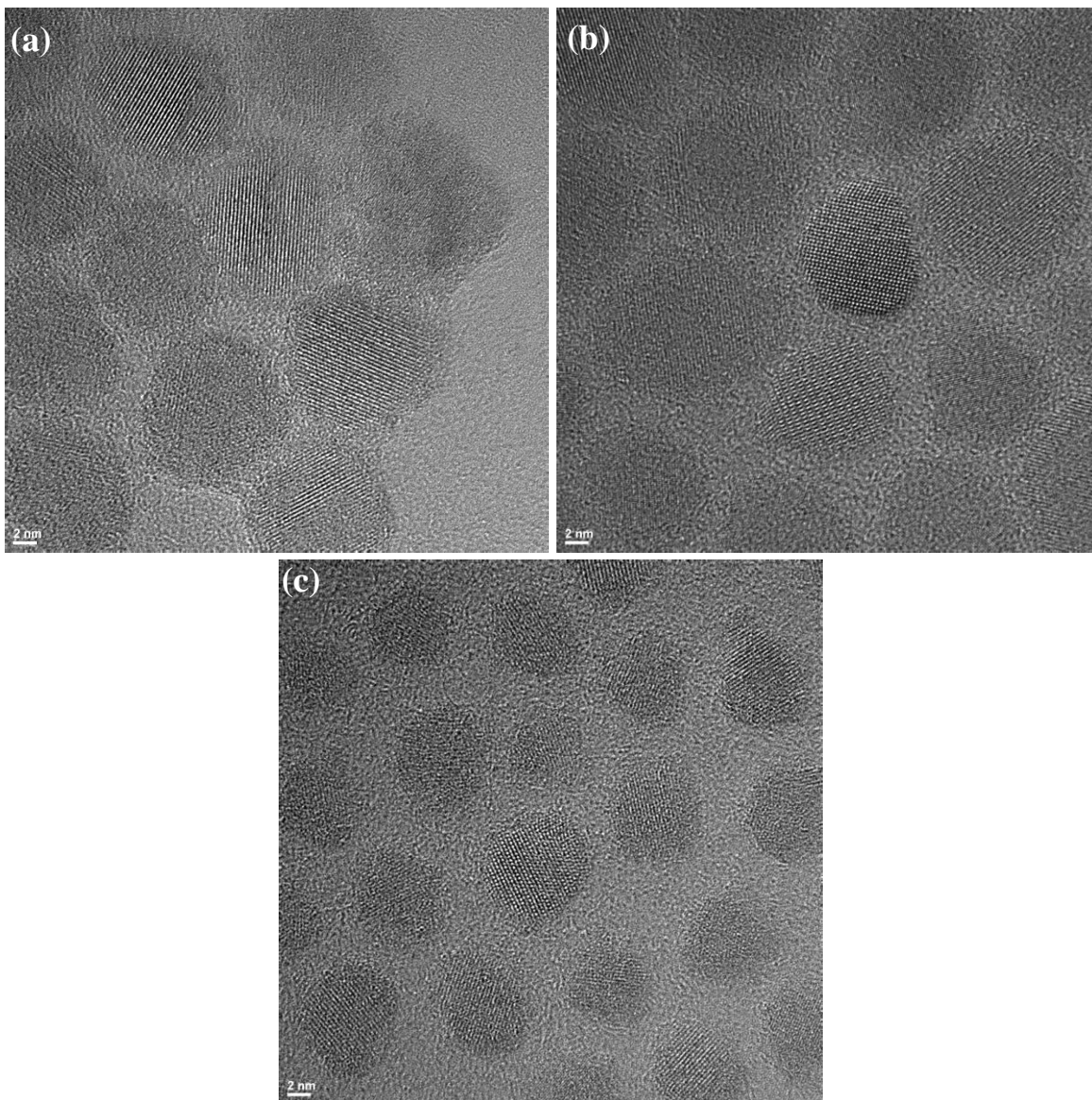


Fig S3. HRTEM images of wurtzite phase (a) CuGaSnS_4 and defect chalcopyrite phase (b) CuInSnS_4 (c) CuGaSnS_4 nanocrystals

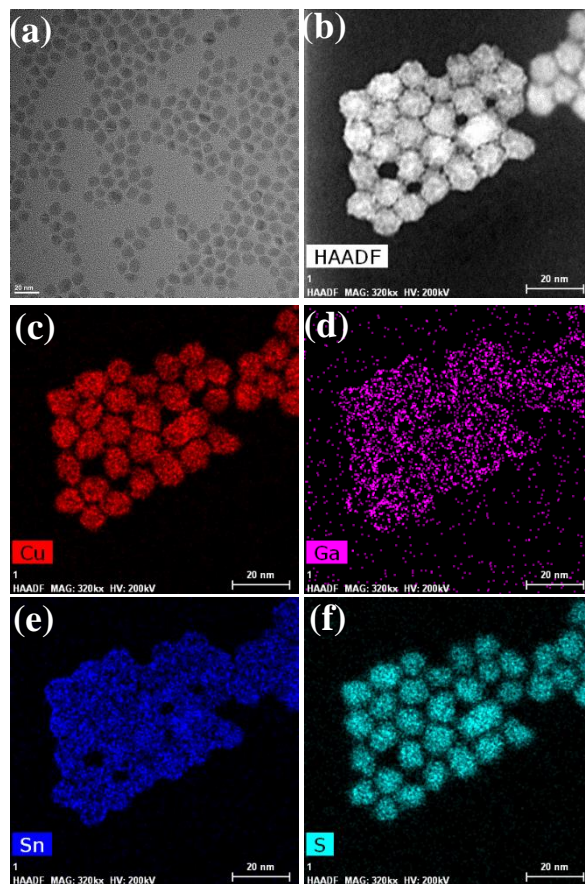


Fig. S4 (a) TEM image of wurtzite phase CuGaSnS_4 nanocrystals. (b) High angle annular dark field image. (c)-(f) STEM-EDX elemental mapping images of Cu, Ga, Sn and S.

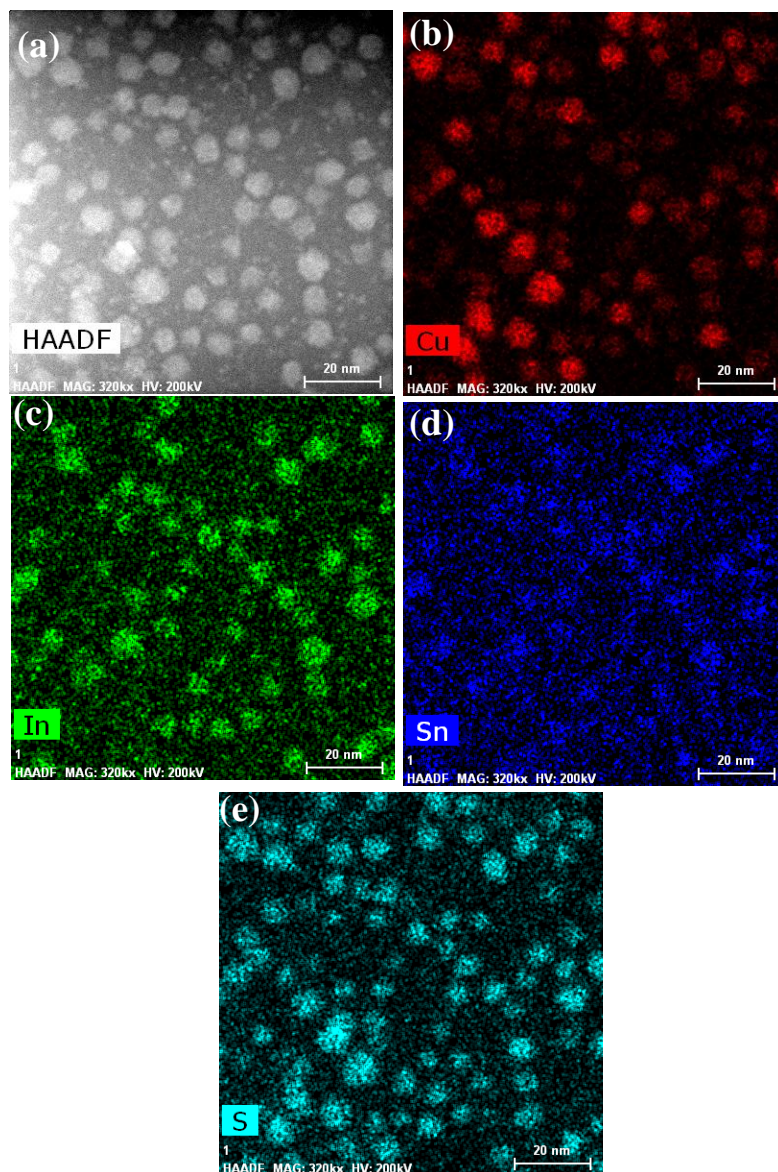


Fig. S5 (a) High angle annular dark field image of defect chalcopyrite phase CuInSnS_4 . (b)-(e) STEM-EDX elemental mapping images of Cu, In, Sn and S.

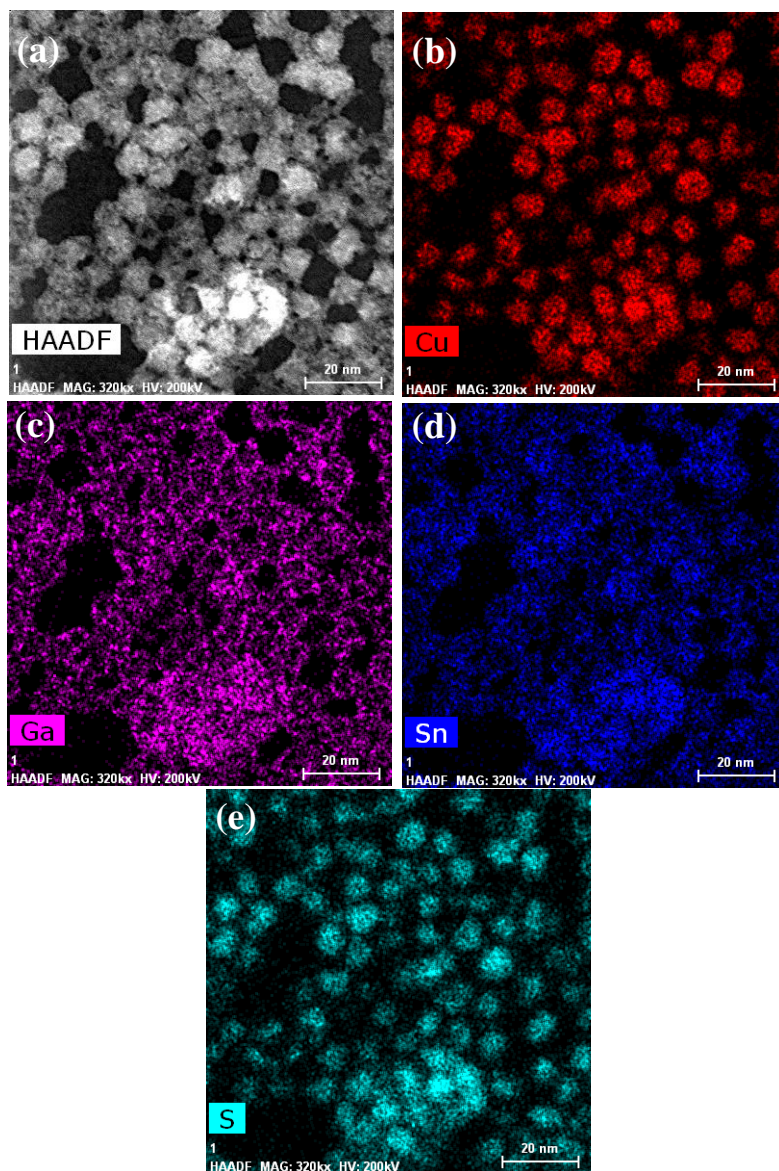


Fig. S6 (a) High angle annular dark field image of defect chalcopyrite phase CuGaSnS_4 . (b)-(e) STEM-EDX elemental mapping images of Cu, Ga, Sn and S.

Table S1. Composition (from EDX Analysis) of CuMSnS₄ (M = In or Ga) nanocrystals with wurtzite and defect chalcopyrite structures.

Compound	Structure	Cu : M : Sn : S	S/(Cu+M+Sn)
CuInSnS ₄	Wurtzite	17.5 : 18.3 : 15.2 : 49.0	0.96
CuGaSnS ₄	Defect Chalcopyrite	17.0 : 16.2 : 18.3 : 48.5	0.94
CuInSnS ₄	Wurtzite	16.7 : 16.6 : 17.2 : 49.5	0.98
CuGaSnS ₄	Defect Chalcopyrite	17.3 : 17.1 : 16.3 : 49.3	0.97

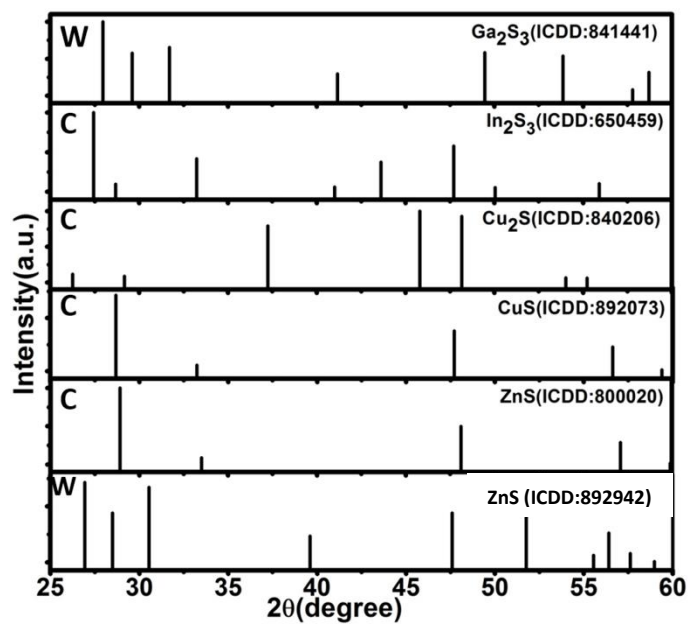


Fig S7. ICDD XRD patterns for related binary phases; W and C represent the wurtzite and cubic phase, respectively.

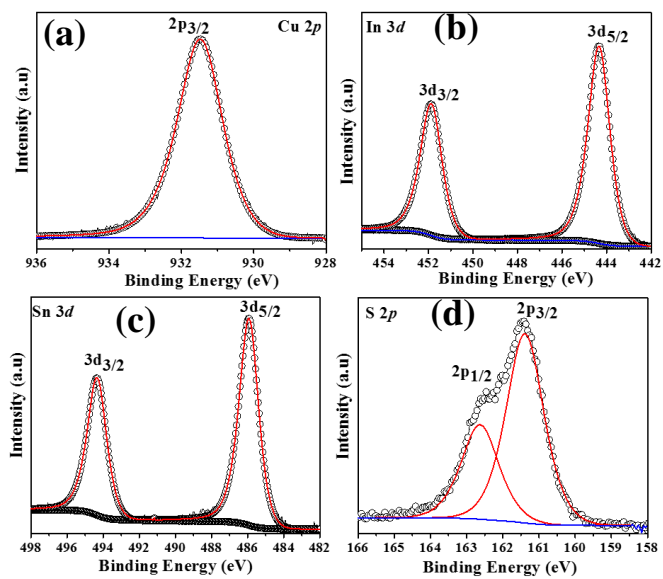


Fig S8. XPS plots of wurtzite phase CuInSnS_4 . (a) Cu_{2p} core-level spectra, (b) In_{3d} core-level spectra, (c) Sn_{3d} core-level spectra, and (d) S_{2p} core-level spectra. Blue lines correspond to background for the different spectra while red lines correspond to fits to the data.

Table S2. Structural and optical properties of various copper-based chalcogenide compounds.

Compound	Crystal Structure	Lattice Constant (Å)	Band Gap (eV)	Ref
CuInS ₂	Tetragonal	5.522 (<i>a</i>): 11.132 (<i>c</i>)	1.53	1, 2
CuGaS ₂	Tetragonal	5.349 (<i>a</i>): 10.468 (<i>c</i>)	2.41	2,3
Cu ₂ ZnSnS ₄	Tetragonal	5.427 (<i>a</i>): 10.871 (<i>c</i>)	1.44 -1.51	4
Cu ₂ FeSnS ₄	Wurtzite	3.856 (<i>a</i>): 6.364 (<i>c</i>)	1.54	5
Cu ₂ CdSnS ₄	Wurtzite	3.821 (<i>a</i>): 6.258 (<i>c</i>)	1.42	6
CuFeS ₂	Tetragonal	5.289 (<i>a</i>): 10.423 (<i>c</i>)	0.5 - 0.6	7
Cu ₂ SnS ₃	Tetragonal	5.412 (<i>a</i>): 10.810 (<i>c</i>)	1.35	8
Cu ₃ SnS ₄	Cubic	5.38 (<i>a</i>)	1.75	9
CuInSnS ₄	Cubic	10.487 (<i>a</i>)	N/A	10
CuGaSnS ₄	Orthorhombic	13.954 (<i>a</i>): 8.886 (<i>b</i>): 6.476 (<i>c</i>)	N/A	11
CuInSnS ₄	Wurtzite	3.895 (<i>a</i>): 6.420 (<i>c</i>)	1.31	This work
CuInSnS ₄	Defect Chalcopyrite	5.511 (<i>a</i>): 11.130 (<i>c</i>)	1.40	This work
CuGaSnS ₄	Wurtzite	3.829 (<i>a</i>): 6.310 (<i>c</i>)	1.17	This work
CuGaSnS ₄	Defect Chalcopyrite	5.416 (<i>a</i>): 10.856 (<i>c</i>)	1.30	This work

1. Kistaiah, P.; Murthy, K. S. *J. Less-Common Met.* **1985**, *105*, 37.
2. Alonso, M. I.; Wakita, K.; Pascual, J.; Garriga, M.; Yamamoto, N. *Phy. Rev. B*, **2001**, *63*, 075203.
3. J.L. Shay, J.H. Wernick, Ternary Chalcopyrite Semiconductors: Growth Electronic Properties and Applications, Pergamon Press, Oxford, 1974.
4. Paier, J.; Asahi, R.; Nagoya, A.; Kresse, G. *Phys. Rev. B.*, **2009**, *79*, 115126.
5. Zhang, X.; Bao, N.; Ramasamy, K.; Wang, Y-H. A; Wang, Y.; Lin, B.; Gupta, A. *Chem. Commun.*, **2012**, *48*, 4956.
6. Li, C.; Cao, M.; Huang, J.; Wang, L. J.; Shen, Y. *Mater. Lett.*, **2015**, 140 170.
7. Wang, Y-H. A.; Bao, N.; Gupta, A. *Solid State Sciences*, **2010**, *12*, 387.
8. Fernandes, P.A.; Salome, P.M. P.; da Cunha, A. F. *J. Phys. D: Appl. Phys.* **2010**, *43*, 215403.
9. Chalapathi, U.; Kishore Kumar, Y.B.; Uthanna, S., Sundara Raja, V.; *Thin Solid Film.*, **2014**, *556*, 61.
10. Mauhl, D.; Pickardt, J.; Reuter, B., *Zeitschrift für Anorganische und Allgemeine Chemie*, **1982**, *491*, 203.
11. Garbato, L.; Geddo-Lehmann, A.; Ledda, F. *J. Cryst. Growth*, **1991**, *114*, 299.